Water Science & Technology

IWA PUBLISHING

Water Science & Technology Vol 85 No 10, 2854 doi: 10.2166/wst.2022.135

Design-oriented evaluation of the hydrodynamics in a full-scale combined filter-lamella separator for urban stormwater treatment

Max Stricker [a,*], Tobias Littfinski[a], Eva Heinz[a], Klaus Hans Pecher[b], Manfred Lübken [a], Helmut Grüning[c] and Marc Wichern [a]

[a] Department of Civil and Environmental Engineering, Institute of Urban Water Management and Environmental Engineering, Ruhr-Universität Bochum, Universitätsstraße 150, Bochum 44801, Germany
[b] Dr. Pecher AG, Klinkerweg 5, Erkrath 40699, Germany
[c] Faculty of Energy, Building Services, Environmental Engineering, University of Applied Sciences Münster, Stegerwaldstraße 39, Steinfurt 48565, Germany
*Corresponding author. E-mail: max.stricker@ruhr-uni-bochum.de

MS, 0000-0003-3306-4441

ABSTRACT

The development of compact treatment devices with high removal efficiencies and low space requirements is a key objective of urban stormwater treatment. Thus, many devices utilize a combination of sedimentation and upward flow filtration in a single system. This study, for the first time, evaluates the flow field inside a combined filter-lamella separator via computational fluid dynamics. Herein, three objectives are investigated: (i) the flow field for different structural configurations, (ii) the distribution of particulate matter along the filter bed and (iii) the dynamic clogging in discrete filter zones, which is addressed by a clogging model derived from literature data. The results indicate that a direct combination of a filtration stage with a lamella separator promotes a uniform flow distribution. The distribution of particulate matter along the filter bed varies with configuration and particle size. Clogging, induced by particles in the spectrum $<63\,\mu m$, creates gradients of hydraulic conductivity along the filter bed. After treating about half of Germany's annual runoff-efficient precipitation at a rainfall intensity of 5 L/(s·ha), the filtration rates increase in the front of the filter bed by $+10\%$. Thus, long-term operating behavior is sensitive to efficient filter utilization in compact treatment devices.

Key words: best management practices, clogging, computational fluid dynamics, filtration, lamella separator, stormwater

HIGHLIGHTS

- A holistic approach is used to capture the system behavior concerning hydrodynamics, filter resistance and filter clogging.
- The filter media improves the distribution of flow in the lamella stage.
- Larger particles utilize only about 50% of the filter area due to inertia effects.
- Gradients of hydraulic conductivity regionally alter filtration rates and flow rates in the inclined plates.

GRAPHICAL ABSTRACT

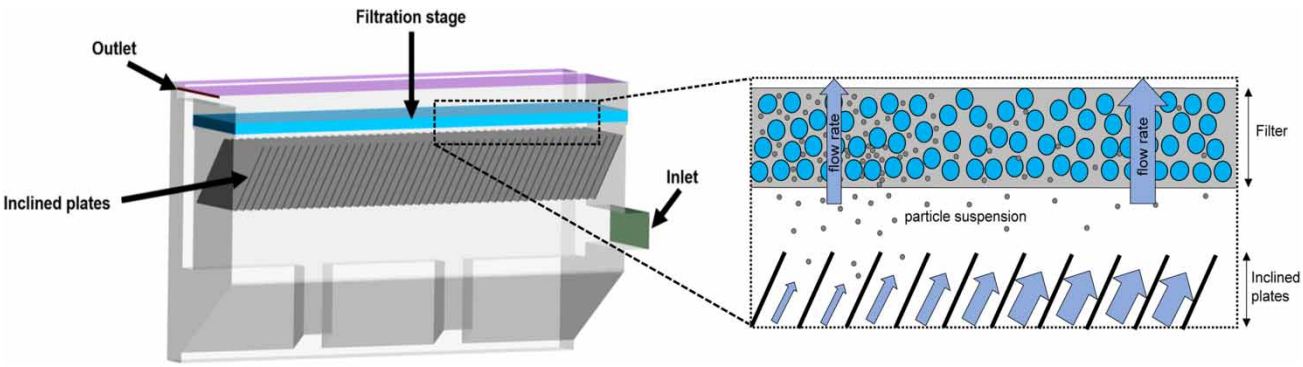

INTRODUCTION

Due to increasing knowledge of pollutant pathways, new urban stormwater management practices have been developed in recent decades, which are referred to throughout the literature as best management practices (BMP), stormwater control measures (SCM) or low impact development (LID) (Fletcher *et al.* 2015). These include compact treatment devices integrated into the underground stormwater sewer system, which treat stormwater in a decentralized or semicentralized manner and often combine a preliminary sedimentation with an upward flow filtration in a single unit (Gruening *et al.* 2011). This combination extends the longevity of a filter by retaining coarse particles in the sedimentation stage (Herr & Sansalone 2015) and is thus also a promising approach for the application on a central scale (Grüning & Schmitz 2018). Overall, the implementation of filter media provides an enhanced removal efficiency with respect to particulate matter (Langeveld *et al.* 2012) and adsorptive-binding pollutants like hydrocarbons and heavy metals (Vesting *et al.* 2015; Okaikue-Woodi *et al.* 2020). Nevertheless, filter media are prone to clogging and therefore require regular maintenance. The service life of a filter until hydraulic failure occurs, i.e. an unacceptable decrease of filter permeability, depends, among other things, on the filter loading rate, the filter grain size and structure, the size of the particles in the stormwater, the influent concentration and filtration rates (Siriwardene *et al.* 2007; Kandra *et al.* 2015). The adsorption ability of a filter medium is generally described by the adsorption capacity and the adsorption kinetics, which are usually derived from laboratory-scale batch tests. Removal rates for a specific pollutant may differ depending on filter medium, initial pollutant concentration, composition of the stormwater, filter loading and contact time (Liu *et al.* 2005; Deng 2020).

In the context of compact treatment devices combining upward flow filtration and sedimentation, not much attention has been paid to the efficient use of the filter area, which depends on the hydrodynamics of the system. To date, explicit research on this topic is rare, except for the study of Pathapati & Sansalone (2009), who indicated a non-uniform filter loading in a radial cartridge filter system. Thereby, the filter surface was only partly utilized by larger particles (75 μm), while smaller particles tended to utilize a larger filter surface. Such circumstances may influence long-term clogging behavior, accelerating the decrease of filter permeability in certain areas. This might also change the underlying flow field of a sedimentation stage and enforce higher filtration rates in specific filter zones, which will diminish the contact time of soluble pollutants in the specific filter areas.

This study aims to showcase these effects and addresses them explicitly by the use of computational fluid dynamics (CFD), which has been applied to a variety of wastewater-related problems (Samstag *et al.* 2016). Herein, the system under investigation is a compact treatment device, which combines a filtration stage with a lamella separator in a single unit. Lamella separators offer great potential concerning the effective removal of particulate matter in a confined space. However, to take advantage of the increased surface area, a uniform surface loading is a prerequisite, which can be constructively challenging (Fuchs *et al.* 2014). CFD simulations of lamella separators concerning potable water and stormwater were performed by some authors with different objectives, e.g. Salem *et al.* (2011); Tarpagkou & Pantokratoras (2014). Tarpagkou & Pantokratoras (2014) followed a macroscopic approach, investigating the overall flow field of a full-scale system with inclined plates. Salem *et al.* (2011) evaluated the flow distribution in a bench-scale model, comparing simulation results to experimental tracer data. However, a lamella separator combined with a filtration stage has not been investigated.

Throughout this study, the optimal configuration of a combined filter-lamella separator for stormwater treatment is examined via CFD with the software ANSYS Fluent. In a first step, different design configurations are examined by altering the angle of inclination of the inclined plates in the lamella separator. Thereby, the design configuration that produces the most uniform flow distribution along the inclined plates is determined. Afterwards, the distribution of particulate matter along the filter bed is evaluated and analyzed concerning different particle diameters. The last objective of this study is to predict the development of dynamic filter clogging with an increasing volume of stormwater treated. Therefore, a simple nonlinear clogging model based on laboratory data of Kandra *et al.* (2015) is applied to predict the decrease of hydraulic conductivity along the filter bed. The distribution of particulate matter, filtration rates and flow rates inside the inclined plates are compared before and after loading about half of Germany's annual runoff-efficient precipitation to the system.

METHODS

System configurations

The system under investigation is a compact treatment device combining a filtration stage and a lamella separator into a single unit, built by Dr. Pecher AG (Erkrath, Germany). In this study, the lamella stage is represented by an inclined plate system

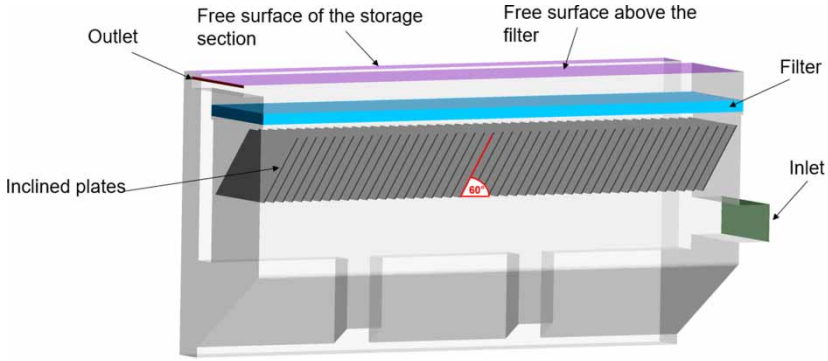

Figure 1 | Combined filter-lamella separator (configuration B). In configuration A the filter is not present. Configuration C contains a filter, but the inclined plates are pointing at a 60° angle towards the inlet.

Table 1 | Dimensions of the combined filter-lamella separator and scenario information

Basin length	7.2 m
Basin width	1.38 m
Basin depth	3.8 m
Number of inclined plates	47
Angle of inclined plates	60°
Filter depth	15 cm
Filter area	10.8 m^2
Number of filter zone divisions	48
Impermeable catchment area	3.8 ha
Total amount of stormwater treated	300 mm
Rainfall intensity	5 L/(s·ha)

with 47 inclined plates. The geometry of the system is depicted in Figure 1. Herein, stormwater enters via the inlet, advances in the main flow direction and passes upwards through the inclined plates. Afterwards, the stormwater percolates through the filter media. The hydraulic head that forces the water through the filter is generated by a rising free water level in the storage section of the system. The storage section is of rectangular geometry and attached to the actual treatment device by three rectangular openings. There are two free surface water levels: (i) above the filter media and (ii) above the storage section. If the pressure drop of the filter media exceeds the design values of the system, untreated stormwater is discharged from the storage section into the receiving water body. In all other cases, treated stormwater passes through the filter and exits the system over a weir. Throughout this study, three design configurations are evaluated: without filtration and inclined plates at a 60° angle pointing against the main flow direction (configuration A), with filtration and inclined plates at a 60° angle pointing against the main flow direction (configuration B) and with filtration and inclined plates at a 60° reversed angle pointing in the main flow direction (configuration C). For an in-depth analysis, the filter is horizontally divided into 48 equally spaced filter zones with a length of 15 cm. This classification allows us to study the development of heterogeneous clogging along the filter bed. Dimensions of the system and scenario information are given in Table 1.

Governing equations of single-phase flow

The Reynolds-Averaged-Navier-Stokes equations (RANS), i.e. conservative equations of mass (Equation (1)) and averaged momentum (Equation (2)), are solved for turbulent flow of an incompressible fluid. In cartesian coordinates they are denoted

as follows:

$$\frac{\partial u_i}{\partial x_i} = 0 \tag{1}$$

$$U_j \frac{\partial U_i}{\partial x_j} = -\frac{1}{\rho}\frac{\partial p}{\partial x_i} + \frac{\partial}{\partial x_j} + \left(v\left(\frac{\partial U_i}{\partial x_j} + \frac{\partial U_j}{\partial x_i}\right) - \bar{u}_i'\bar{u}_j' \right) \tag{2}$$

where p is the static pressure, v is the kinematic viscosity, u_i denotes the instantaneous velocity associated with the x_i coordinate, while U_i is the average mean flow velocity and u_i' is the turbulent velocity fluctuation such that $u_i = U_i + u_i'$. The term $\bar{u}_i'\bar{u}_j'$, which is known as the Reynolds-stress tensor, has to be modeled by a turbulence closure model. In the case of k-ε RANS models, turbulence closure models include transport equations for k (turbulent kinetic energy) and ε (dissipation) and the concept of eddy viscosity, which is depicting turbulence by a gradient-diffusion term (Ferziger & Perić 2002). Concerning k-ε models, different model variations exist, namely Standard, Re-Normalisation Group (RNG) and the Realizable k-ε model (ANSYS Inc. 2020). In this study, turbulence in the liquid phase was modeled by the RNG k-ε model, which was used by Tarpagkou & Pantokratoras (2014) in a previous study of a large-scale lamella separator. Moreover, Tarpagkou & Pantokratoras (2014) validated the RNG k-ε model within the ANSYS Fluent code environment with Laser Doppler velocimetry velocity measurements in a rectangular sedimentation tank (Liu *et al.* 2010). The transport equations for k and ε are as follows:

$$\frac{\partial}{\partial x_i}(\rho k u_i) = \frac{\partial}{\partial x_i}\left(a_k \mu_{eff}\frac{\partial k}{\partial x_j}\right) + G_k + G_b - \rho\varepsilon \tag{3}$$

$$\frac{\partial}{\partial x_i}(\rho \varepsilon u_i) = \frac{\partial}{\partial x_i}\left(a_k \mu_{eff}\frac{\partial \varepsilon}{\partial x_j}\right) + C_{1\varepsilon}\frac{\varepsilon}{k}(G_k + C_{3\varepsilon}G_b) - C_{2\varepsilon}\rho\frac{\varepsilon^2}{k} - R_\varepsilon \tag{4}$$

where G_k is the generation of turbulence kinetic energy due to mean velocity gradients, G_b is the generation of turbulence kinetic energy due to buoyancy, a_k and a_ε are inverse Prandtl numbers for k and ε equation, respectively, μ_{eff} is the effective viscosity, and $C_{1\varepsilon}$, $C_{2\varepsilon}$ and $C_{3\varepsilon}$ are turbulence model constants. The term R_ε in the ε equation accounts for the effects of streamline curvature and rapid strain. Further information on the model can be found in the ANSYS Fluent Theory Guide (ANSYS Inc. 2020). Detailed information on the derivation of turbulence models and the concept of eddy viscosity is depicted in Ferziger & Perić (2002). To enable a step-wise mesh refinement a scalable wall function was used, similar to the modeling approach of Salem *et al.* (2011).

Modeling was done under steady-state conditions on a 3D geometry; see Figure 1. Regarding the simulation set-up for single-phase flow, the following boundary conditions have been applied: The inlet was defined as a 'velocity inlet' with 0.0275 m/s, representing an average rainfall intensity of 5 L/(s·ha). The overflow of the weir was represented by a 'pressure outlet' condition. Both free water surfaces were set up as shear-free 'symmetry' boundary conditions. All physical walls were defined as 'no slip' boundary conditions.

Governing equations of the secondary phase

In this simulation, an Euler-Lagrangian approach is applied to model the particle behavior, which is also referred to as Discrete Phase Model (DPM). This approach neglects interaction between particles, i.e. collision and agglomeration during the stormwater event. As the probability of particles colliding decreases with low particulate volume fractions (PVF), it is only valid for very dilute multiphase flows with a PVF smaller than 10^{-3} (Elghobashi 1991). Concerning the characteristics of particulate matter of the sample location, the PVF in the influent, without considering a further dilution by the stored water volume in the system, is significantly lower (in the order of 10^{-5}). It is also assumed that the impact of the particles on the fluid phase by momentum exchange is negligible at the present volume fractions and particle sizes. This approach was used in previous stormwater-related studies, and led to sufficient agreement between simulated and experimental results within computationally reasonable limits (Pathapati & Sansalone 2009). Therefore, a one-way coupling scheme was used, which limits the momentum exchange in one direction, i.e. particles are affected by the fluid phase but not vice versa. This means that the fluid phase can be solved in the absence of the particles to find the steady-state solution of the flow

field. Then particles are released from the inlet and their motion is calculated by a stepwise integration of the force balance:

$$m_p \frac{du_p}{dt} = F_D + F_g + F_a \tag{5}$$

where m_p=mass of particle; u_p=particle velocity; F_D=drag force; F_g=gravitational force; F_a=additional forces (e.g. virtual mass and lift force). Additional forces are not considered in this simulation. The gravitational force F_g accounts for reduced gravity by buoyance and is calculated as follows:

$$F_g = m_p \frac{g(\rho_p - \rho)}{\rho_p} \tag{6}$$

where g=gravitational acceleration; ρ_p=particle density; ρ=fluid density. The drag force F_D is calculated as follows:

$$F_D = m_p \frac{18\mu\ C_D Re_p}{\rho_p d_p^2\ 24} \tag{7}$$

where μ=dynamic viscosity of the fluid; Re_p=particle Reynolds number; d_p=particle diameter; C_D=drag force coefficient. The drag force coefficient is calculated by the empirical model of Morsi & Alexander (1972) assuming the particle to be spherical. Generally, this assumption may not be valid for particles originating from abrasive processes; however, the effect of irregular shape has only a minor influence on the settling behavior of small particles (Rommel *et al.* 2020). Hence, the model is considered suitable for the scope of this investigation. Stochastic tracking was chosen for modeling turbulent dispersion of particles accounting for velocity fluctuations of turbulent flow.

A 'reflect' boundary condition was utilized at all physical wall boundaries. Particles reaching the filter media were trapped with a 'trap' boundary condition at the downward-facing surface of the filter zones. Therefore, the trajectories of particles that are not removed by sedimentation end at the downward-facing filter surface. For each of the 48 filter zones, mass loading rate and particle size can be individually determined. This approach allows an evaluation of the distribution of particulate matter among the filter bed surface, which gives information about the utilization of the filter area. As particles either were trapped on the filter surface or remained in the system, an 'escape' boundary condition was not used. The removal criteria of Pathapati & Sansalone (2009) were adopted for this study: In a first run, the tracking length of neutrally buoyant particles was determined. The tracking length after which at least 95% of the neutrally buoyant particles reached the filter bed was then used as a removal criterion for all particles. Thus, any particle that was still in the system after the tracking length had expired was considered to be removed.

Modeling filter media

The filter media was modeled by a porous media approach adding an additional momentum source term to the momentum equations in the assigned cells. The source term for isotropic porous media is as follows (ANSYS Inc. 2020):

$$S_i = -\left(\frac{\mu}{\alpha} u_i + C_2 \frac{1}{2} \rho |u| u_i\right) \tag{8}$$

comprising a viscous loss term $\mu/\alpha u_i$ and an inertial loss term $C_2 1/2 \rho |u| u_i$. Where α=permeability; u_i=superficial velocity; C_2=inertia resistance coefficient. Since the Reynolds number in the filter media (Re≈3.5) is less than 10, which marks the beginning of a transition from viscous- to inertia-dominated flow, inertial losses were neglected. Therefore, Equation (8) corresponds to Darcy's Law expressed in terms of permeability α. However, more commonly Darcy's Law is expressed in terms of hydraulic conductivity k_f, which denotes the ability of a filter media to transmit water. Permeability α and hydraulic conductivity k_f can be transferred into each other as follows:

$$k_f = \frac{\rho g}{\mu} \alpha \tag{9}$$

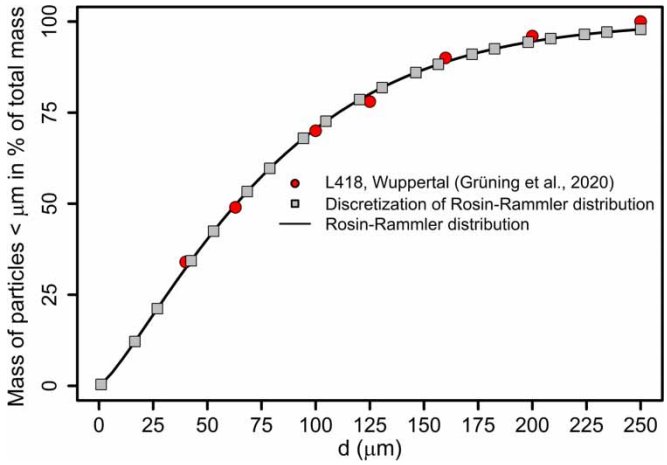

Figure 2 | Sieved road dust, Rosin-Rammler distribution and discretized particle size distribution of road dust from the catchment site (L418, Wuppertal, Germany).

where k_f=hydraulic conductivity (m/s). Throughout this study, the ability of the filter media to transmit water is denoted in terms of hydraulic conductivity, as it is the commonly used parameter for stormwater filtration.

Particle properties in the catchment area

The properties of particulate matter were adopted from Grüning *et al.* (2020), who took samples of road dust from the catchment area (L418, Wuppertal, Germany) of the system under investigation. Thereby, an average particle density of 2.58 g/cm^3 and the particle size distribution (PSD) were determined by sieving. It was hypothesized that only particles ≤250 µm were of relevant size to impact on the filter loading. Hence, the PSD was limited to fractions of d_{max} ≤250 µm. To provide an approximate distribution of particulate matter in between the sieving classes and below 40 µm, a Rosin–Rammler distribution was fitted to the data. A Rosin–Rammler distribution is a common representation of a PSD and is expressed as follows:

$$Y_d = 1 - e^{-(d/\bar{d})^n} \tag{10}$$

where Y_d is the mass fraction of particles smaller than d (µm); $\bar{d}$ (µm) and n (–) are fitting parameters representing the mean diameter and spread parameter, respectively. Values after fitting by root mean squared error (RMSE)-criterion (R^2=0.98) to experimental data were 85 µm and 1.25 for $\bar{d}$ and n. With respect to the findings of Dickenson & Sansalone (2009), who evaluated the influence of PSD discretization in DPM simulations, the Rosin–Rammler distribution was discretized into 20 diameter classes. These diameter classes were used to represent the PSD of road runoff in the carried-out simulations. The diameter classes, Rosin–Rammler distribution and the raw data are depicted in Figure 2. The concentration of total suspended solids (TSS) in the road runoff was assumed to be 150 mg/L at the inlet of the lamella separator (Kayhanian *et al.* 2012).

Prediction of filter clogging

A simple nonlinear clogging model was derived from literature data to account for filter clogging within the 48 subdivisions of the filter bed. In the context of stormwater filtration, several authors have focused on modeling mechanical clogging, e.g. Siriwardene *et al.* (2007); Wang *et al.* (2012); Tang *et al.* (2020). However, the prediction of filter clogging is complex and depends on a set of parameters; therefore, different clogging phenomena (deep bed filtration and surface filtration) are observed within different experiments. Table 2 shows a selection of studies, which were considered as input data for the prediction of the filter clogging. Herein, the type of filtration corresponds to the observed clogging phenomena. However, a clear distinction is sometimes not possible, as mechanisms of deep bed filtration and surface filtration can take place simultaneously. Therefore, only the predominant filtration type is depicted. In this study, suitable data for the prediction of clogging was selected from the literature based on the expected ratio of particle size and filter grain size, which was found to be an important parameter impacting the nature of clogging (Herzig *et al.* 1970; Kandra *et al.* 2015).

For the simulation, it is hypothesized that the usual filter grain size of granular filter media with adsorption capability may range from 0.5 to 2.5 mm (Vesting *et al.* 2015). The size of particles reaching the filter bed is evaluated using DPM

Table 2 | Overview of pre-selected filtration studies for stormwater treatment

Particle size	Filter grain size	Predominant filtration type	References
d_{50}=25–65 μm	0.215 mm	Surface filtration	Siriwardene *et al.* (2007)
d_{50}=25–65 μm	10.5 mm	Deep bed filtration	Siriwardene *et al.* (2007)
50–75 μm	0.1–0.25 mm	Surface filtration	Wang *et al.* (2012)
d_{max}<75 μm d_{50}=31 μm	2–2.36 mm	Deep bed filtration	Kandra *et al.* (2015)
d_{50}=470 μm	D_{50}=2.03 mm	Surface filtration	Tang *et al.* (2020)
d_{max}<125 μm d_{50}=63 μm	20 mm	Deep bed filtration	Conley *et al.* (2020)

simulations. Due to the assigned 'trap' boundary condition, the trajectories of particles that are not removed by sedimentation end at the downward-facing surface of the filter zones. Each filter zone is then evaluated according to filter load and particle size. In this process, only particles <66 μm reach the filter bed and are therefore considered to be involved in the clogging. Thus, a simple clogging model was derived from the experimental data of Kandra *et al.* (2015), which fitted well within the assumed size constraints. Herein, the clogging of granular zeolite filter media was evaluated by particles <75 μm. The filter grain used passed a 2.36 mm sieve and was retained on a 2 mm sieve. The sediment was taken from a stormwater pond and dosed stepwise into a laboratory filter column. The accumulation of particles was fairly constant across layers, indicating a deep bed filtration. Over time, a decrease of infiltration rate was observed with an increasing volume of stormwater treated. This data was extracted by Web Plot Digitizer (https://automeris.io/WebPlotDigitizer/) and used to predict the decrease of hydraulic filter performance in terms of hydraulic conductivity k_f and filter load M within this simulation. Further information on the derivation of the clogging model is depicted in the supplementary information of this publication. The decrease of hydraulic conductivity was described as a nonlinear function:

$$k_f = k_{f,I} \cdot e^{-a \cdot M} \tag{11}$$

where k_f=hydraulic conductivity (m/s); $k_{f,I}$=initial hydraulic conductivity of an unloaded filter (m/s); a = model parameter (m^2/kg); M = filter load (kg/m^2). Note that filter load M is defined as the mass of particulate matter that was dosed to the experimental filter column, related to the area of the filter surface. The best fit of the nonlinear function to the experimental data was observed for $a = 0.023$ (RMSE-criterion, $R^2 = 0.88$). In the present study, the initial hydraulic conductivity of an unloaded filter was assumed to be $1.4 \cdot 10^{-2}$ m/s with a filter bed depth of 15 cm. At the given volume flow rate this complies to a differential pressure of roughly 2 cm water column height. However, a decrease of hydraulic conductivity or an increase of volume flow rate will increase the differential pressure observed and can be calculated according to Equations (8) and (9).

Simulation procedure for dynamic filter clogging

To account for a gradual development of clogging, an iterative filter loading procedure is used; see Figure 3. Firstly, the hydraulic conductivity is defined for each of the 48 filter zones. Starting with an unloaded filter, an initial hydraulic conductivity of $1.4 \cdot 10^{-2}$ m/s is assigned to each filter zone. Thereafter, the flow field of the single-phase flow is computed. In a third step, particulate matter is injected into the inlet and tracked through the system, eventually hitting the filter bed or being removed by sedimentation. Particulate matter reaching the filter bed is counted with respect to its mass and spatial distribution on the surfaces of the filter zones. Practically, the first run of the simulation procedure depicts a lamella-filter separator that has just been put into operation: The filter is not yet loaded, and particles that enter the system utilize the filter bed according to the established flow field and particle properties. On this basis mass loading rate $\dot{m}_i$ (kg/s) is calculated for each filter zone i. After a specific amount of stormwater V_S is treated, the resulting filter load M_i, i.e. the mass of particulate matter entering the filter zone related to its surface area, is then calculated for every filter zone i as follows:

$$M_i = \frac{\dot{m}_i}{Q} \cdot \frac{A_C}{A_{F,i}} \cdot (V_S \cdot 10^4) \tag{12}$$

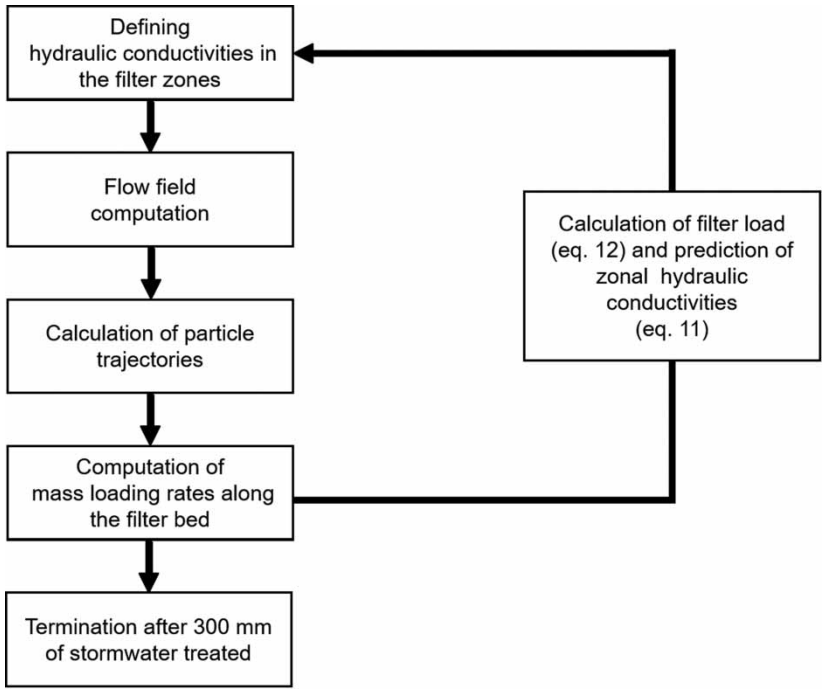

Figure 3 | Simulation procedure for the prediction of dynamic filter clogging.

where M_i = filter load of i^{th} filter zone (kg/m^2); Q = total volume flow rate (L/s); A_C = catchment area of the system (ha); $A_{F,i}$ = surface area of i^{th} filter zone (m^2) and V_S = stormwater precipitation height per catchment surface area (mm). The factor 10^4 is a conversion factor (L/ha·mm). However, with increasing filter load M_i, new hydraulic conductivities are calculated by Equation (11) for each filter zone and are updated within the CFD simulations. At this point, the calculation of the flow field and particle trajectories is recalculated. This procedure allows us to account for changes in the flow field caused by gradual and heterogeneous clogging of the filter bed. In this iterative manner, the system was loaded five times starting with an unloaded system (0 mm of stormwater treated). The first four loading steps contained 50 mm and the last step 100 mm of stormwater. Therefore, the cumulative amount of stormwater treated by the system was 50 mm, 100, 150, 200 and 300 mm, which corresponds to about half of Germany's annual runoff-effective precipitation. Note that the simulations were carried out under steady state conditions with a constant rainfall intensity of 5 L/(s·ha). The timing of termination was primarily chosen due to increasing uncertainties in the clogging model.

Convergence criteria and discretization

Convergence criteria was based on scaled residuals dropping below 10^{-3} and velocities, which were monitored at different locations throughout the domain. The solution was considered to be converged when scaled residuals and monitored velocities were stable and did not change during further iterations. In all simulations a second order discretization scheme was used. For pressure-velocity coupling the SIMPLE-algorithm was selected. The influence of grid refinement was investigated using three meshes with increasing number of cells. The grid refinement study was carried out on configuration B. Meshes under investigation had 3,025,762, 5,623,125 and 12,819,821 elements for coarse, medium and fine mesh, respectively. In Figure 4 the mean velocities in the cross-sections of the inclined plates are depicted for different meshes. As the results from the medium sized mesh are in good agreement with the fine mesh, the medium sized mesh was selected for all simulations due to lower computing time.

RESULTS AND DISCUSSION

Hydraulics of a combined filter-lamella separator for stormwater treatment

In configuration A, stormwater is distributed unevenly along the inclined plates; see Figure 5 for flow field and Figure 6 for absolute flow rates. Herein, about 68% of the incoming stormwater passes through the last ten inclined plates. The maximum

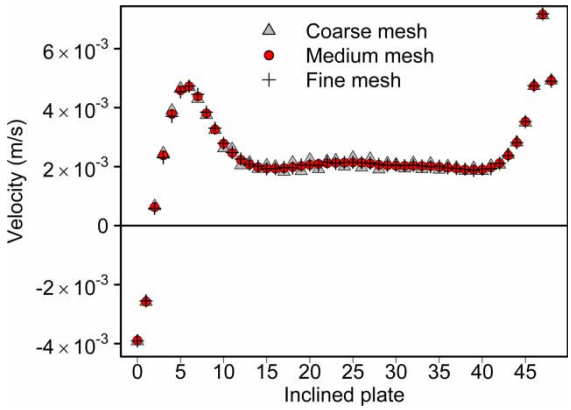

Figure 4 | Mean velocities in the cross-section of the inclined plates obtained on different meshes from single-phase flow simulations. Simulations were carried out on configuration B. Inclined plates are numbered in ascending order starting from the inlet of the system.

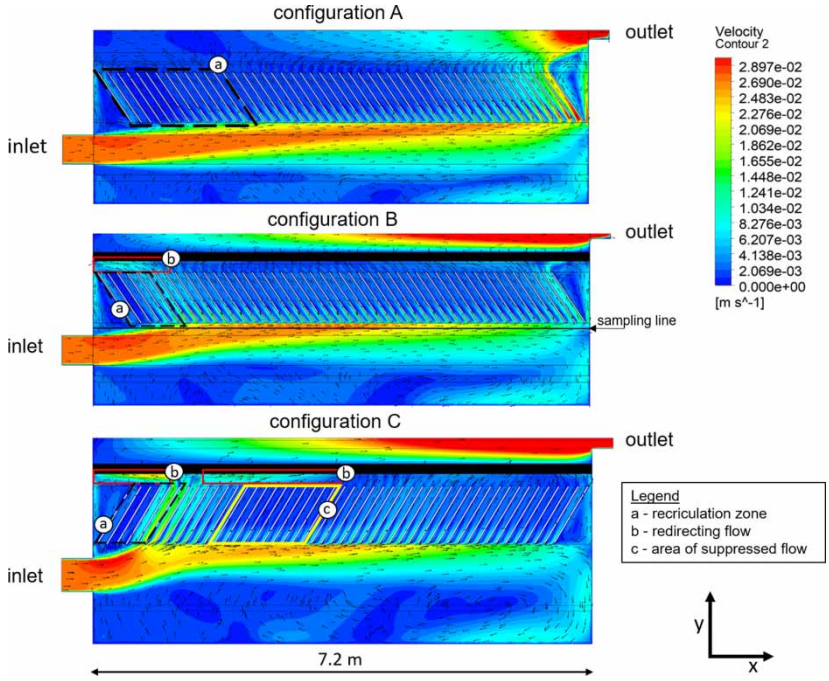

Figure 5 | Velocity fields in the vertical cross-section of different configurations under steady-state conditions at constant rainfall intensity of 5 L/(ha·s). The black bar above the inclined plates represents the filter.

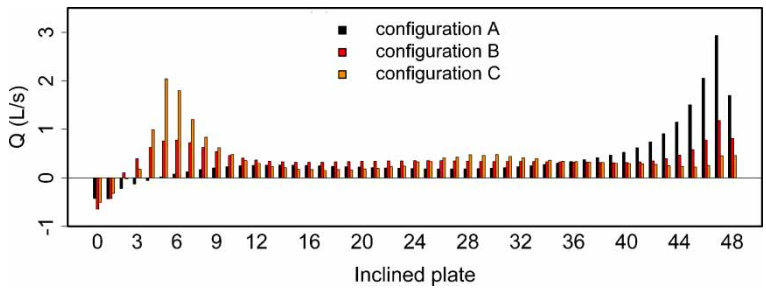

Figure 6 | Flow rate Q in the inclined plates for different system configurations. Inclined plates are numbered in ascending order starting from the inlet of the system.

flow rate was 2.80 L/s in the 46th plate, corresponding to a surface loading of 14.82 m/h with respect to its horizontally projected surface area. Simultaneously, a recirculation zone is established in the vicinity of the inlet, which is accompanied by negative flow rates in the first set of plates, see Figure 5 (configuration A, black dotted box).

In configuration B, stormwater is almost evenly distributed along the inclined plates. Herein, a maximum flow rate of about 1.18 L/s is established in the 46th plate, corresponding to a specific surface loading of 6.24 m/h. Despite the mainly uniform distribution, two zones of slightly higher flow-through form: One in the last set of plates at the end of the building (40th–47th plates), which is already present in configuration A, and a new one, in the vicinity of the inlet (3rd–10th plates); see Figures 5 and 6. A recirculation zone is present up to the fifth inclined plate; see Figure 5 (black dotted box). Above the plates with high flow rates, a redirecting flow is formed; see Figure 5 (red box). In this case, the flow rates exceed the local hydraulic capacity of the filter in this area. Hence, stormwater is forced to enter the filter somewhere else and is redirected into other filter areas.

Configuration C demonstrated that the angle of inclined plates strongly influences the flow field. Herein, high flow rates are established in the 5th–9th plates, transporting about 30% of the incoming stormwater. The maximum flow rate is 2.00 L/s in the 5th plate, corresponding to a surface loading of 10.58 m/h. Above the plates with a high surface loading, strong redirecting flows develop. These are characterized by stormwater that is redirected into neighboring filter zones, which is noticeable by the increased flow velocities in the space between the inclined plates and the filter; see Figure 5 (red boxes). Areas of suppressed flow velocities occur below filter zones that are loaded by stormwater from strong redirecting flows; see Figure 5 (yellow box). However, when the loading by the redirected stormwater ceases, the flow rates in the underlying plates increase again. Likewise, in configuration B, a recirculation zone forms in the first plates (1st–5th plates); see Figure 5 (black dotted box).

Comparing the design configurations A, B and C, an overall improvement is observed by the combination of a filtration stage with a lamella separator. Thereby, the resistance of the filter reduces the maximum observed flow rates in specific plates and promotes a uniform surface loading (configurations A, B and C). However, different flow fields develop by altering the angle of the plates (configurations B and C). In contrast to configuration B, configuration C exhibits a strong shortcutting flow in the first set of plates. This difference may be explained by the increased shear in configuration B in comparison to a reduced shear in configuration C. In configuration C, the plates point in the main flow direction, reducing the overall shear and making the first set of plates directly accessible to stormwater. Thus, the highest flow rates develop in the front of the system. In configuration B, the plates are inclined against the main flow direction, exerting additional shear to the flow, which finally reduces the flow rates in the inclined plates. In both configurations, the interaction of inclined plates and the filter media creates redirecting flows. In configuration C, these pose an additional problem as the redirecting flows suppress the flow rates in the underlying plates, favoring a non-uniform distribution. It is hypothesized that these redirecting flows result from a filter resistance, whose influence does not extend far enough into the flow field of the lamella separator. Thus, a direct vertical connection of plates and filter media might extend this influence, as it prohibits the compensation of pressure gradients along the filter bed by redirecting flows and thereby enforces a uniform surface loading of the inclined plates. Recirculation zones form in all design configurations. However, the presence of a filter media reduces the size of the recirculation zone from 13 to 5 inclined plates from configuration A to B and C, respectively.

Distribution of particulate matter on the filter bed

The distribution of particulate matter on the filter bed, i.e. the utilization of the filter area by particles, is firstly determined for configurations B and C with a yet unloaded filter. In configuration B a nearly uniform distribution of particles develops along the filter bed. A slightly increased utilization of the filter bed emerges in the rear part (6 m and beyond) and the midsection (3.2–4.8 m). The front of the filter bed (0–1.2 m) is reached by slightly fewer particles. The distribution of particulate matter along the filter bed for configuration B with an unloaded filter (0 mm of stormwater) is depicted in Figure 7 (red curve). In configuration C, a heterogeneous distribution of particulate matter along the filter bed can be observed, elevating an early clogging in the front of the filter bed. Herein, about 36 weight-% of the particles utilize the area from 0.8 m to 2.4 m of the filter bed length, while only 17 weight-% utilize the rear part (5.6 m–7.2 m). In the former case, there will be higher maintenance requirements with respect to the specific area. The distribution of particulate matter along the filter bed for configuration C with an unloaded filter (0 mm of stormwater) is depicted in Figure 7 (yellow curve).

For an in-depth insight, the distribution of particulate matter on the filter bed is studied for different particle diameters (20 μm, 30 μm, 40 μm) for design configuration B. Thereby, it is found that 40 μm particles predominantly hit the filter bed in the rear part, while 20 and 30 μm particles are almost evenly distributed along the filter bed; see Figure 8. Further

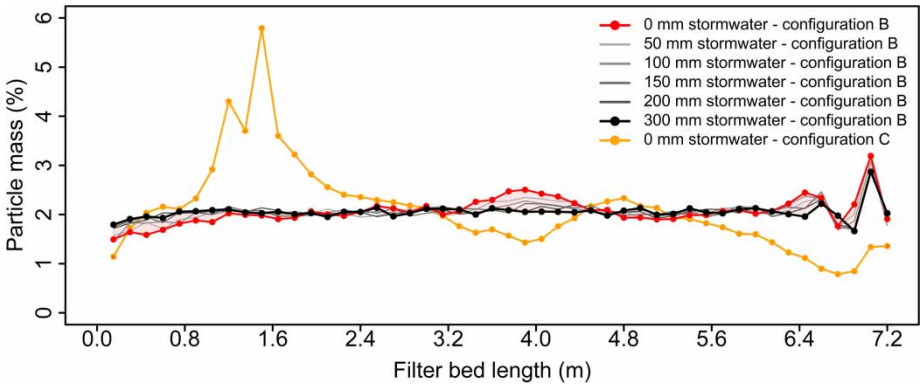

Figure 7 | Distribution of particulate matter on the filter bed for different design configurations (B and C) and loading steps (0–300 mm of cumulative stormwater) at constant rainfall intensity of 5 L/(s·ha). The length of the filter bed is counted upwards from the inlet.

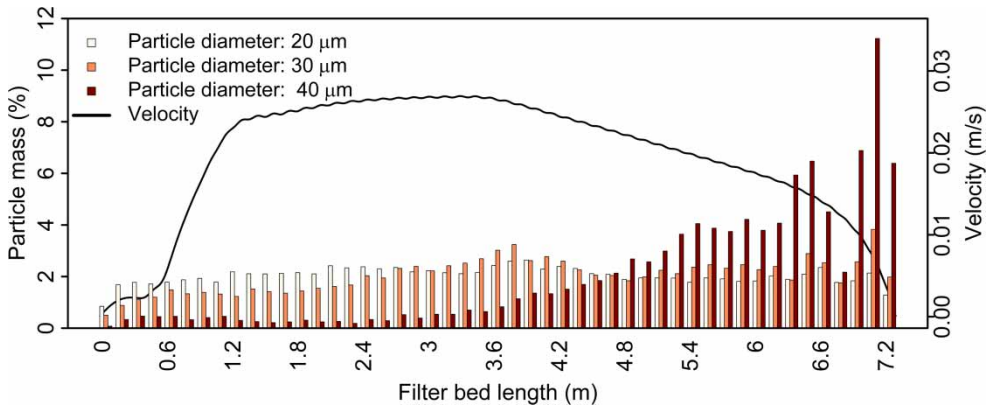

Figure 8 | Distribution of particulate matter with different particle diameters along the filter bed and velocity component in the main flow direction (in x-direction) from a sampling line 5 cm underneath the inclined plates in configuration B (see Figure 5 for coordinates and location of the sampling line). The length of the filter bed is counted upwards from the inlet.

understanding of the filter utilization can be achieved by plotting the velocity component in the main flow direction from underneath the inclined plates. The velocity component in the main flow direction (x-direction) was sampled from a sampling line 5 cm underneath the plates; see Figure 5. Along the sampling line, the velocity component in x-direction increases rapidly from 0 to 0.02 m/s (0–1.2 m), remains relatively stable (1.2–3.6 m), and decreases again from 0.025 to 0 m/s (3.6–7.2 m); see Figure 8. Simultaneously, the decrease of velocity in x-direction coincides with an increase of particles with a diameter of 40 μm entering the filter bed (3.6 m and beyond). Conversely, the distribution of particles with a diameter of 20 or 30 μm is not significantly impacted. This observation is related to the different particle masses. Particles with high mass experience higher inertial forces when trying to follow the imposed flow of an inclined plate. Thus, they require sufficiently low velocities to leave the main flow and move upward through an inclined plate. An exception is made for areas where the main flow is not yet attached to the inclined plates. Consequently, 40 μm particles do not utilize the front of the filter bed, even if velocities are low. The results indicate that an estimation of filter utilization by particulate matter may be misleading if it is based on single-phase flow or soluble tracer data only.

Dynamic filter clogging

The development of heterogeneous, dynamic filter clogging is investigated for design configuration B, as it was the best configuration regarding an even surface loading of the inclined plates and the distribution of particulate matter on the filter bed. The aim is to investigate how the flow field and the distribution pattern of particulate matter change with an increasing amount of stormwater treated. Over the course of treating 300 mm of stormwater, 1,710 kg of particles $\leq$250 μm were injected into the inlet, which is about half of the expected annual material removal from the catchment area. From these, 452 kg of particles $\leq$66 μm reached the filter bed. The filter load was calculated after each loading step (50 mm, 100 mm,

150 mm, 200 mm, 300 mm) and for each of the 48 filter zones. In between these loading steps, the hydraulic conductivity was updated and the described simulations steps were repeated; see section *Simulation procedure for dynamic filter clogging*. In Figure 9 the results of the simulation procedure are shown.

After the treatment of 300 mm of stormwater the predicted filter load is on average 42 kg/m^2; see Figure 9(a). An overall low filter load is established in the front of the filter bed (0 m–1.2 m), ranging from 30 kg/m^2 to about 42 kg/m^2. In the midsection (3.2 m–4.6 m) a slightly higher filter load develops with a maximum of 45 kg/m^2 at around 3.7 m. In the rear part (6 m–7.2 m) the highest filter load is 60 kg/m^2 in a single filter zone. Conceivably, the observed filter loads qualitatively match with the observed distribution of particulate matter along the filter bed; see Figures 7 and 9(a). However, a comparison of the distribution patterns after each loading step indicated a change of filter utilization. Thereby, zones with initially high utilization gradually decrease and zones with initially low utilization increase with an increasing volume of stormwater treated; see Figure 7 (red, grey and black curves). This redistribution can be attributed to the formation of hydraulic conductivity gradients in the filter bed. These gradients locally enhance or diminish filtration rates and thereby influence the flow field and the distribution of particulate matter along the filter bed. Nevertheless, the influence of the redistribution is too weak to change the overall pattern of filter load, which does not even out significantly; see Figure 9(a). Over the course of dosing 300 mm of stormwater, the hydraulic conductivity of an unloaded filter gradually decreases from 1.4×10^{-2} m/s to an average of 5×10^{-3} m/s; see Figure 9(b). An overall high hydraulic conductivity develops in the front of the filter bed, ranging from 6.25 to 5×10^{-3} m/s. Below-average hydraulic conductivities are observed in the midsection and lower hydraulic conductivities in the rear part, with a minimum of 2.6×10^{-3} m/s.

As expected, the gradients of hydraulic conductivity moderate the filtration rates Q_{Filter}, i.e. the amount of water which flows through the surface area of a specific filter zone. Thus, high filtration rates emerge in filter zones with high and low filtration rates in filter zones with small hydraulic conductivities; see Figure 10(a). Especially in the front (0 m–1.2 m), the midsection (3.2 m–4.6 m) and the rear part (6 m–7.2 m), the filtration rates significantly deviate from filtration rates in an unloaded filter bed (0 mm of stormwater); see Figure 10(a). Remarkably, in the front, filtration rates increase from 1.75 L/(s·m^2) to a maximum of 2.18 L/(s·m^2), with an overall total increase of +10%.

It is hypothesized that the filtration rates also impact on the flow rates in the underlying inclined plates. Therefore, the relative change of the flow rates in the inclined plates $\Delta Q/Q_0$ is calculated from two different scenarios: (i) configuration B with 300 mm of stormwater treated and (ii) configuration B with 0 mm of stormwater (unloaded filter). Thereby, ΔQ corresponds to the absolute difference in flow rates at 0 mm and 300 m of stormwater treated. Q_0 corresponds to the flow rates in the inclined plates with an unloaded filter. Thus, $\Delta Q/Q_0 > 0$ coincides with an increase and $\Delta Q/Q_0 < 0$ with a decrease of flow rate; see Figure 10(b). Consistently with the high filtration rates, the flow-through in the inclined plates increases in the front of the system. Thereby, the highest relative increase in flow rate is observed in the third inclined plate with about +46%. In total, flow rates in the first six plates increase by +16%. In the midsection and the rear part of the inclined plates the flow-through decreases, which is attributed to the decreased filtration rates in these regions.

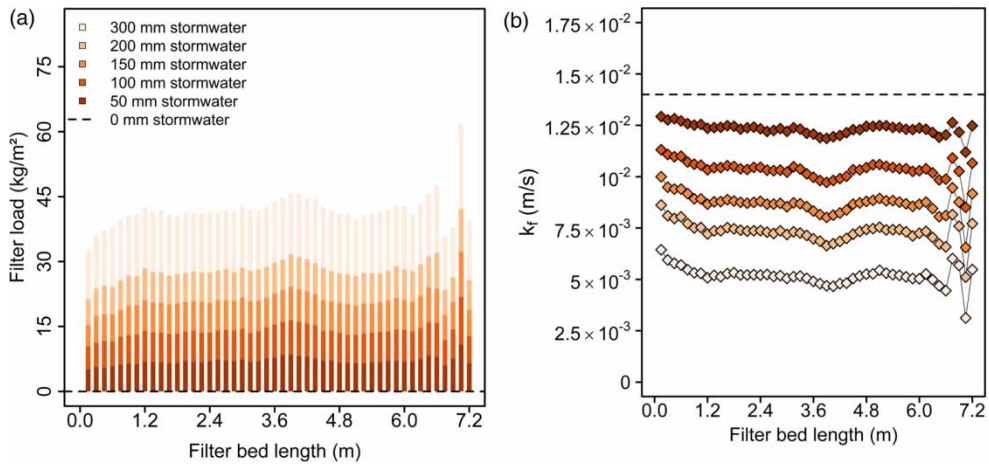

Figure 9 | (a) Development of filter load and (b) hydraulic conductivity k_f along the filter bed (b) after the treatment of different volumes of stormwater. Simulations were carried out on configuration B. The length of the filter bed is counted upwards from the inlet.

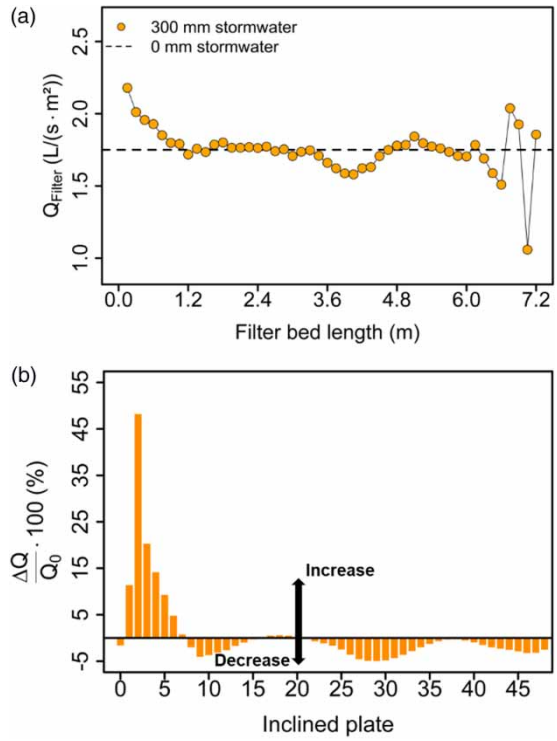

Figure 10 | (a) Filtration rate Q_{Filter} by filter area before and after the treatment of 300 mm of stormwater. (b) Relative change of flow rates in the underlying inclined plates $\Delta Q/Q_0$. Simulations were carried out on configuration B. Inclined plates are numbered in ascending order starting from the inlet of the system.

CONCLUSIONS

In the present study, the hydrodynamics in a combined filter-lamella separator with upward flow filtration was investigated by numerical simulations. Contrary to a lamella separator without filtration stage, the peak flow rate in the inclined plates drops from 2.80 L/s (without filter) to a minimum of 1.18 L/s when a filter is present. In the latter, the best flow situation in terms of flow distribution is achieved by inclined plates pointing at an 60° angle against the main flow direction. Mainly particulate matter in the spectrum $\leq$63 µm reaches the filter bed and is considered to be involved in the filter clogging. However, larger particles (40 µm) predominantly utilize the rear part of the filter bed, using only 50% of the complete filter area. After the treatment of about half of Germany's runoff-effective precipitation, the hydraulic conductivity of the filter bed decreases from 1.4×10^{-2} to an average of 5×10^{-3} m/s. Thereby, gradients of hydraulic conductivity form along the filter bed, increasing filtration rates in specific areas of the filter from 1.75 L/(s·m^2) to a maximum of 2.18 L/(s·m^2). In these areas, the retention of pollutants by filter-adsorption processes will likely suffer from an increased load and a simultaneously shortened hydraulic retention time. Thus, the long-term operating behavior of compact treatment devices requires the best possible utilization of the complete filter area. Compact treatment devices with modular filter systems might offer a flexible exchange of clogged filter media, restoring functionality and saving filter substrate. In this case, CFD simulations can provide valuable information regarding optimized design and operational behavior. However, additional future on-site or laboratory investigations of these systems will be necessary to complement the findings from CFD simulations.

ACKNOWLEDGEMENTS

This work was supported by the Ministry for Culture and Science of the State of North-Rhine Westphalia (NRW, Germany) through the joint project 'Future Water' (project number: 321-8.03-215-116439).

DATA AVAILABILITY STATEMENT

All relevant data are included in the paper or its Supplementary Information.

REFERENCES

ANSYS Inc. 2020 *ANSYS Fluent Theory Guide R1*.

Conley, G., Beck, N., Riihimaki, C. A. & Tanner, M. 2020 Quantifying clogging patterns of infiltration systems to improve urban stormwater pollution reduction estimates. *Water Research X* **7**, 100049. doi:10.1016/j.wroa.2020.100049.

Deng, Y. 2020 Low-cost adsorbents for urban stormwater pollution control. *Frontiers of Environmental Science & Engineering* **14**, 5. doi:10.1007/s11783-020-1262-9.

Dickenson, J. A. & Sansalone, J. J. 2009 Discrete phase model representation of particulate matter (PM) for simulating PM separation by hydrodynamic unit operations. *Environmental Science & Technology* **43** (21), 8220–8226. doi:10.1021/es901527r.

Elghobashi, S. 1991 Particle-laden turbulent flows: direct simulation and closure models. *Applied Scientific Research* **48**, 301–314.

Ferziger, J. H. & Perić, M. 2002 *Computational Methods for Fluid Dynamics*, 3rd, rev. edn. Springer Berlin Heidelberg, Berlin, Heidelberg, s.l.

Fletcher, T. D., Shuster, W., Hunt, W. F., Ashley, R., Butler, D., Arthur, S., Trowsdale, S., Barraud, S., Semadeni-Davies, A., Bertrand-Krajewski, J.-L., Mikkelsen, P. S., Rivard, G., Uhl, M., Dagenais, D. & Viklander, M. 2015 SUDS, LID, BMPs, WSUD and more – The evolution and application of terminology surrounding urban drainage. *Urban Water Journal* **12** (7), 525–542. doi:10.1080/1573062X.2014.916314.

Fuchs, S., Mayer, I., Haller, B. & Roth, H. 2014 Lamella settlers for storm water treatment – performance and design recommendations. *Water Science & Technology* **69** (2), 278–285. doi:10.2166/wst.2013.698.

Gruening, H., Hoppe, H., Messmann, S. & Giga, A. 2011 Cost effectiveness of centralised and decentralised storm water treatment. *Water Science & Technology* **63** (11), 2598–2604. doi:10.2166/wst.2011.163.

Grüning, H. & Schmitz, T. 2018 Teil 2: Systeme zur technischen Regenwasserfiltration: Kennwerte und Bemessung. (Part 2: technical rainwater filtration: key figures and dimensioning). *GWF-Wasser/Abwasser* **159** (3), 63–69.

Grüning, H., Wichern, M., Pecher, K., Schmitz, T., Heinz, E., Evers, M. & Böckmann, D. 2020 *Analyse und Optimierung des Rückhalts von feinpartikulären und gelösten Stoffen in Anlagen zur technischen Regenwasserfiltration (ReWaFil I). (Analysis and Optimisation of the Retention of Fine Particulate and Dissolved Substances in Plants for Technical Rainwater Filtration)*. Report for the Ministry for Environment, Agriculture, Conservation and Consumer Protection of the State of North Rhine-Westphalia (MULNV), Germany.

Herr, C. & Sansalone, J. J. 2015 In situ volumetric filtration physical model to separate particulate matter from stormwater. *Journal of Environmental Engineering* **141** (9), 4015017. doi:10.1061/(ASCE)EE.1943-7870.0000946.

Herzig, J., Leclerc, D. & Le Goff, P. 1970 Flow of suspensions through porous media, application to deep filtration chemistry. *Journal of Industrial and Engineering Chemistry* **62** (5), 8–35.

Kandra, H., McCarthy, D. & Deletic, A. 2015 Assessment of the impact of stormwater characteristics on clogging in stormwater filters. *Water Resources Management* **29** (4), 1031–1048. doi:10.1007/s11269-014-0858-x.

Kayhanian, M., McKenzie, E. R., Leatherbarrow, J. E. & Young, T. M. 2012 Characteristics of road sediment fractionated particles captured from paved surfaces, surface run-off and detention basins. *The Science of the Total Environment* **439**, 172–186. doi:10.1016/j.scitotenv.2012.08.077.

Langeveld, J. G., Liefting, H. J. & Boogaard, F. C. 2012 Uncertainties of stormwater characteristics and removal rates of stormwater treatment facilities: implications for stormwater handling. *Water Research* **46** (20), 6868–6880. doi:10.1016/j.watres.2012.06.001.

Liu, D., Sansalone, J. J. & Cartledge, F. K. 2005 Comparison of sorptive filter media for treatment of metals in runoff. *Journal of Environmental Engineering* **131** (8), 1178–1186. doi:10.1061/(ASCE)0733-9372(2005)131:8(1178).

Liu, B., Ma, J., Luo, L., Bai, Y., Wang, S. & Zhang, J. 2010 Two-dimensional LDV measurement, modeling, and optimal design of rectangular primary settling tanks. *Journal of Environmental Engineering* **136** (5), 501–507. doi:10.1061/(ASCE)EE.1943-7870.0000186.

Morsi, S. A. & Alexander, A. J. 1972 An investigation of particle trajectories in two-phase flow systems. *Journal of Fluid Mechanics* **55** (02), 193. doi:10.1017/S0022112072001806.

Okaikue-Woodi, F. E. K., Cherukumilli, K. & Ray, J. R. 2020 A critical review of contaminant removal by conventional and emerging media for urban stormwater treatment in the United States. *Water Research* **187**, 116434. doi:10.1016/j.watres.2020.116434.

Pathapati, S.-S. & Sansalone, J. J. 2009 CFD modeling of particulate matter fate and pressure drop in a storm-water radial filter. *Journal of Environmental Engineering* **135** (2), 77–85. doi:10.1061/(ASCE)0733-9372(2009)135:2(77).

Rommel, S. H., Gelhardt, L., Welker, A. & Helmreich, B. 2020 Settling of road-deposited sediment: influence of particle density, shape, low temperatures, and deicing salt. *Water* **12** (11), 3126. doi:10.3390/w12113126.

Salem, A. I., Okoth, G. & Thöming, J. 2011 An approach to improve the separation of solid-liquid suspensions in inclined plate settlers: CFD simulation and experimental validation. *Water Research* **45** (11), 3541–3549. doi:10.1016/j.watres.2011.04.019.

Samstag, R. W., Ducoste, J. J., Griborio, A., Nopens, I., Batstone, D. J., Wicks, J. D., Saunders, S., Wicklein, E. A., Kenny, G. & Laurent, J. 2016 CFD for wastewater treatment: an overview. *Water Science & Technology* **74** (3), 549–563. doi:10.2166/wst.2016.249.

Siriwardene, N. R., Deletic, A. & Fletcher, T. D. 2007 Clogging of stormwater gravel infiltration systems and filters: insights from a laboratory study. *Water Research* **41** (7), 1433–1440. doi:10.1016/j.watres.2006.12.040.

Tang, Y., Yao, X., Chen, Y., Zhou, Y., Zhu, D. Z., Zhang, Y., Zhang, T. & Peng, Y. 2020 Experiment research on physical clogging mechanism in the porous media and its impact on permeability. *Granular Matter* **22**, 2. doi:10.1007/s10035-020-1001-8.

Tarpagkou, R. & Pantokratoras, A. 2014 The influence of lamellar settler in sedimentation tanks for potable water treatment – a computational fluid dynamic study. *Powder Technology* **268**, 139–149. doi:10.1016/j.powtec.2014.08.030.

Vesting, A., Heinz, E., Helmreich, B. & Wichern, M. 2015 Removal of hydrocarbons from synthetic road runoff through adsorptive filters. *Water Science & Technology* **72** (5), 802–809. doi:10.2166/wst.2015.285.

Wang, Z., Du, X., Yang, Y. & Ye, X. 2012 Surface clogging process modeling of suspended solids during urban stormwater aquifer recharge. *Journal of Environmental Sciences* **24** (8), 1418–1424. doi:10.1016/S1001-0742(11)60961-3.

First received 26 January 2022; accepted in revised form 11 April 2022. Available online 21 April 2022